Formation of mixed bond-angle linkages in zinc boromolybdate glasses

Margit Fabian[1,2*], Erzsebet Svab[2]

[1]*Centre for Energy Research, Budapest 1121, Hungary*

[2]*Wigner Research Centre for Physics, Budapest 1121, Hungary*

Abstract

The short and medium range structure of glassy MoO_3-ZnO-B_2O_3 has been studied by neutron diffraction and reverse Monte Carlo simulation. The partial atomic pair correlation functions and coordination numbers are presented, not yet reported for this system. We have established that the first neighbor distances do not depend on concentration within limit of error, the actual values are r_{B-O}=1.38 Å, r_{Mo-O}=1.72 Å and r_{Zn-O}=1.97 Å. It is found that ZnO takes part in the glassy structure as network former, as ZnO_4 tetrahedral are linked both to MoO_4 and to BO_3 and BO_4 groups. It is revealed that BO_4/BO_3 increases with increasing B_2O_3 content. We have found that only small amount of boroxol ring is present, BO_3 and BO_4 groups are organized into superstructure units, and a small part is in isolated BO_3 triangles. The BO_3 and BO_4 units are linked to MoO_4 or ZnO_4 forming mixed [4]Mo-O-[3]B, [4]Mo-O-[4]B, [4]Mo-O-[4]Zn, [3]B-O-[4]Zn, [4]B-O-[4]Zn bond-linkages.

1. Introduction

Zinc boromolybdate materials are known as low melting dielectric materials and they have high potential in several applications, due to their stable and unique structure with favourable optical properties [1 and references therein]. The glass formation tendency of MoO_3-ZnO-B_2O_3 and of several other similar compositions has been explored and the optical spectroscopic features have been analyzed by Dimitriev et al. [1-8]. The structure characterization is challenging, as far as this system contains the conditional network former MoO_3 and the traditional network former B_2O_3. For B_2O_3– based glasses it is widely accepted that the network consists of BO_3 and BO_4 groups [9-17], however, the question often arises concerning the relative amount of the trigonal and tetrahedral units. The basic network former units in MoO_3–based glasses are MoO_4 tetrahedral, however, for systems with high concentration (> 80 mol %) both MoO_4 and MoO_6 units are present [3, 18-20]. Several studies deal with ZnO containing glassy systems, concerning the role of Zn^{2+} cations, which may act as modifier if its fraction is low or network former in case of relatively high content of ZnO [1, 21-25].

The glassy $xMoO_3$-$50ZnO$-$(50-x)B_2O_3$ (x=10, 20, 30 mol %) have been prepared and thoroughly investigated using various optical spectroscopic methods and DTA [1]. Concerning the structural characteristics it was found, that the molybdenum-based glasses contain mainly Mo^{6+} ions and a small amount of Mo^{5+} ions might be present. It was found, that the coordination state of Mo^{6+} ions is mainly $(MoO_4)^{2-}$ tetrahedral units, and formation of diborate, triborate and tetraborate groups, which contain BO_3 triangles and BO_4 tetrahedra was also suggested.

In order get deeper insight into the network structure, including the inter-atomic distances and coordination distributions, we have undertaken neutron diffraction study combined with reverse Monte Carlo (RMC) modeling [26] on the same system. Our interest is mainly focused on the

---

* Corresponding author email: fabian.margit@energia.mta.hu

characterization of the network former structural units and their bond-linkages forming the medium-range order. Especially interesting question is the role of ZnO, whether it acts as modifier or network former, not yet investigated for this system, as far as we know.

For the qualitative characterization of the glassy state Transmission Electron Microscopy (TEM) has been performed and Nuclear Magnetic Resonance (NMR) spectroscopy was applied to get complementary information on the boron environment.

2. Experimental

2.1. Sample preparation

The amorphous $xMoO_3$-50ZnO-(50-x)B_2O_3, x=10, 20, 30 mol % samples have been prepared by L. Alexandrov [1]. Commercial powders of reagent grade MoO_3, ZnO and B_2O_3 were used as starting materials and were mixed in an alumina mortar. For this study B_2O_3 was isotopically enriched in [11]B-isotope (99.6%) in order to reduce the influence of the high neutron absorption of [10]B-isotope present in natural boron. For the NMR experiment also [11]B-isotope is needed to get good NMR signals. The homogenous oxide materials were melted at 1200-1250°C in platinum crucible. The glasses were obtained by pouring the melts onto an iron plate and by pressing with another iron plate, for more details see ref [1].

2.2. Transmission electron microscopy

Transmission electron microscopy (TEM) measurements have been carried out with a JEM-ARM 200F analytical electron microscope installed at the National Institute of Materials Physics, Bucharest [27]. Images were recorded at magnifications between 30 000-1 200 000.

2.3. Nuclear Magnetic Resonance measurements

Nuclear Magnetic Resonance (NMR) experiments have been performed with an NMR MAGIC spectrometer operating at 600 MHz installed in the Slovenian NMR Centre [28].

2.4. Neutron diffraction experiments

Neutron diffraction (ND) experiments were performed on the PSD diffractometer (λ_0=1.068 Å) [29] at the 10 MW Budapest research reactor in the momentum transfer range Q=0.5-10 Å^{-1} using the data for preliminary data analysis. The 7C2 diffractometer at the LLB-CEA-Saclay (λ_0 = 0.726 Å) [30] was used in a broader Q-range up to 16 Å^{-1}. The powder specimens of about 3–4 g/each were filled in thin walled cylindrical vanadium sample holder of 8 mm and 6 mm diameter, respectively. Data were corrected for detector efficiency, background scattering and absorption effects. The total structure factor, $S(Q)$ was calculated by local software packages.

3. Experimental results

3.1. Transmission Electron Microscopy analysis

The homogeneity of the glasses was controlled by TEM imaging. According to the TEM observations, no crystallization or phase separation was detected for the studied samples, as illustrated in Figure 1.

Figure 1. TEM images of $30MoO_3$-50ZnO-20B_2O_3 glassy sample.

3.2. Nuclear Magnetic Resonance results

Figure 2 displays the experimental ^{11}B NMR spectra. Two characteristic distributions have been detected: the first one at 1.72 ppm peak position and a broad distribution between 7-20 ppm. Based on the literature (see Figure 1 in [16] and [17]) they are related to [4]B(BO_4) and [3]B(BO_3) structural units, as indicated in Figure 2. The peak intensities show slight, but significant concentration dependence. The intensity of the [3]B peak increases with decreasing boron content, while the [4]B peak decreases. The coordination numbers were calculated simple by integrating the area under these two distributions. The average B-O coordination numbers are 3.26, 3.24 and 3.21 atoms for the 40, 30 and 20 mol% B_2O_3 content samples, respectively. The maximal change is only ~1.5 %, but NMR is a highly sensitive method for the investigation of first neighbor oxygen coordination of [11]B-isotope. The [3]B peak is obviously a double peak with peak positions at 15.3 and 13.3 ppm, indicating two types of symmetry positions. Detailed analysis of the NMR experiment is underway, and will be published elsewhere.
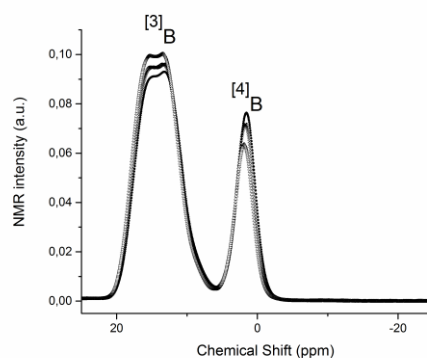

Figure 2. ^{11}B NMR spectra of zinc boromolybdate glasses: $10MoO_3$-$50ZnO$-$40B_2O_3$(dots), $20MoO_3$-$50ZnO$-$30B_2O_3$(cross) and $30MoO_3$-$50ZnO$-$20B_2O_3$ (triangle).

3.3. Neutron diffraction results

Figure 3 presents the total structure factor, *S(Q)* for the investigated zinc boromolybdate glasses. The results of the reverse Monte Carlo model calculation are also drawn in the same figure; they will be discussed later, in Section 4.
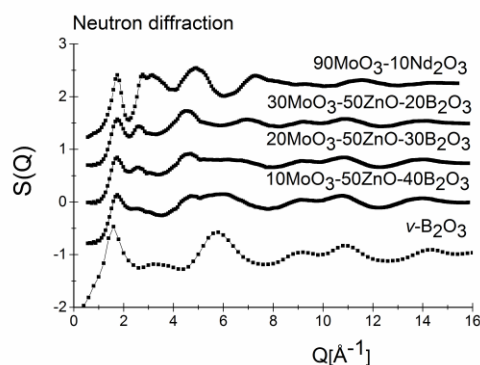

Figure 3. Neutron diffraction structure factor, S(Q) of ternary zinc boromolybdate samples. The binary *v*-B_2O_3 [13] and $90MoO_3$-$10Nd_2O_3$ [18] glasses are also displayed to help the interpretation of the observed chages: experimental data (marks) and RMC simulation solid line (The curves are shifted vertically for clarity).

Significant concentration dependence may be observed. The most striking features are the decrease of the peak intensities at ~2.5, ~4.5 and ~7 Å^{-1}, and the increase of the peak intensity at around 6 Å^{-1}

with decrease of MoO_3/B_2O_3 fraction (see from top to down). The actual peak positions are also shifted. In order to find support for the interpretation, we have displayed the $S(Q)$ data for the binary v-B_2O_3 [13] and $90MoO_3$-$10Nd_2O_3$ [18], as they are the constituent network formers of the investigated ternary system. The basic tendency of the concentration dependence may be related to the characteristic features of the binary glasses, like the presence of the characteristic large peak at 5.8 Å^{-1} in the $S(Q)$ of v-B_2O_3 or the characteristic peak at 4.9 and 7.3 Å^{-1} for $90MoO_3$-$10Nd_2O_3$ glass. It can be established, however, that the $S(Q)$ curves of the presently investigated ternary system are far not the weighted sum of the corresponding binary systems, which predicts a continuous network instead of separation of the two glassy networks. Due to the continuous change of the characteristic features of the $S(Q)$ pattern, the basic atomic scale characteristic features are expected to be preserved, while the main question is, how these units are connected to each other.

The characteristic features of the ternary glasses may be interpreted taking into consideration the different weighting factors, w_{ij} of the partial structure factors, $S_{ij}(Q)$ contributing to the total $S(Q)$. In this work the following formalism is used:

$$S(Q) = \sum_{i,j}^{k} w_{ij} S_{ij}(Q), \tag{1}$$

$$w_{ij} = \frac{c_i c_j b_i b_j}{\left[\sum_{i,j}^{k} c_i b_j \right]^2}, \tag{2}$$

where c_i, c_j are the molar fractions of the components, b_i, b_j the coherent neutron scattering amplitude [31] and k is the number of elements in the sample. The actual w_{ij} values for the investigated ternary samples are tabulated in Table 1.

Table 1. Weighting factors, w_{ij}(%) of the partial structure factors, $S_{ij}(Q)$ and atomic pair-correlation functions, $g_{ij}(r)$.

Sample	Weighting factors, w_{ij}(%)									
	Atom pairs									
	Mo-O	Zn-O	B-O	O-O	Mo-Mo	Mo-Zn	Mo-B	Zn-Zn	Zn-B	B-B
$10MoO_3$-$50ZnO$-$40B_2O_3$	3.74	15.80	29.54	32.22	0.10	0.91	1.72	1.94	7.25	6.78
$20MoO_3$-$50ZnO$-$30B_2O_3$	7.95	16.90	23.63	34.42	0.45	1.96	2.74	2.08	5.81	4.06
$30MoO_3$-$50ZnO$-$20B_2O_3$	12.82	18.00	16.88	36.84	1.11	3.14	2.94	2.20	4.13	1.94

In order to get qualitative and some quantitative information for the local structure we have calculated the total atomic distribution function, $G(r)$ by sine-Fourier transformation as follows:

$$G(r) = \frac{2}{\pi} \int_{o}^{Q_{max}} Q[S(Q)-1]\sin Qr \, dQ, \tag{3}$$

where Q_{max} is the upper integration limit.

Figure 4 displays the $G(r)$ functions of the investigated zinc boromolybdate glasses, and also for the binary systems, with the aim to find the contribution of the actual atom pairs.

Vertical arrow lines indicate the atom pair positions, which were possible to identify. These are the B-O distribution with peak position at 1.38 Å, which appears separately from the other distributions, as its value is significantly lower. Mo-O and Zn-O distributions overlap with each other, centered at 1.75-1.95 Å.
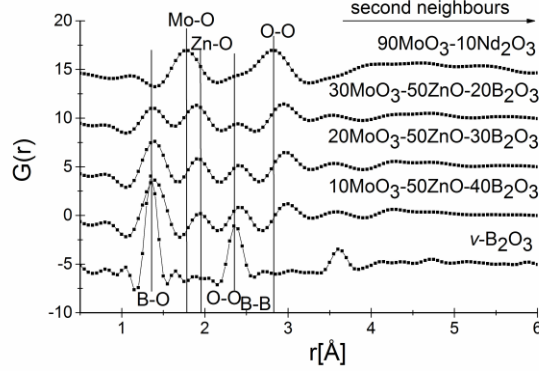
Figure 4. Total distribution functions, *G(r)* calculated by eq. 3 (see text) from *S(Q)* presented in Figure 3. (The curves are shifted vertically for clarity).

Note, that the weight of $G_{Zn-O}(r)$ is significantly higher than that for $G_{Mo-O}(r)$ in the $10MoO_3$-$50ZnO$-$40B_2O_3$ sample (see Table 1), therefore it is possible to identify. The peak at 2.4 Å relates mainly to the $G_{O-O}(r)$, which is a characteristic distance for the BO_3 units and overlaps with $G_{B-B}(r)$ [13]. The peak at ~2.8 Å is related to O-O distance characteristic for Mo-centered oxygen neighborhoods [18]. For higher *r*-values the various atomic distributions overlap with each other, the only small peak at 3.6 Å may be related to the B-O$_{second}$ distance in a BO_3 unit type configuration, as it was identified in *v*-B_2O_3 [13], which is used as a reference sample to analyze the ternary compositions. All these atomic distance values present valuable new information; furthermore, they serve as input parameters for the starting atomic configuration for the RMC modeling.

4. Reverse Monte Carlo modeling

4.1. RMC simulation details

The neutron diffraction experimental *S (Q)* data have been simulated by the RMC method [26], which is a widely used effective tool to model disordered structures. The RMC minimizes the squared difference between the experimental *S(Q)* and the calculated one from a 3-dimensional atomic configuration. The RMC algorithm calculates the one-dimensional partial atomic pair correlation functions $g_{ij}(r)$, and they are inverse Fourier transformed to calculate the partial structure factors, $S_{ij}(Q)$:

$$S_{ij}(Q) = 1 + \frac{4\pi\rho_0}{Q} \int_0^{r_{max}} r\big[g_{ij}(r) - 1\big]\sin Qr \, dr, \qquad (4)$$

where r_{max} is the half edge-length of the simulation box. The atomic configuration of this computer calculation is modified by moving the atoms randomly until the calculated *S(Q)* (see eqs.(1-4)) agrees with the experimental data within the experimental error.

In this study we have used the software package RMC++ developed by Pusztai et al. [32]. For the RMC starting model a random atomic configuration was built up with a simulation box containing 10 000 atoms with density data 0.087, 0.081 and 0.076 atoms·Å^{-3} [1, 33] and half-box values r_{max}=24.30 Å, 24.90 Å and 25.43 Å for the $10MoO_3$-$50ZnO$-$40B_2O_3$, $20MoO_3$-$50ZnO$-$30B_2O_3$ and $30MoO_3$-$50ZnO$-$20B_2O_3$ samples, respectively. In the RMC simulation procedure constraints have been used for the minimum interatomic distances between atom pairs (cut-off distances) to avoid unreasonable atom contacts. The starting cut-off distances have been taken from the experimental *G(r)* function (see Figure 4) as discussed in Section 3.3. and from our previous study [18]. Several RMC runs have been performed by modifying slightly the cut-off distances in the way, that the results of each run have been carefully checked to obtain reliable data for each $g_{ij}(r)$ and coordination number distributions. For each sample about twenty RMC configurations were obtained with more than 2 200 000 accepted moves of atoms.

The convergence of the RMC calculation was good and the final $S(Q)$ matched very well the experimental structure factor as it is shown in Figure 3. The actual set of cut-off distances used in the final RMC run was the following: B-O 1.15 Å, Mo-O 1.6 Å, Zn-O 1.9 Å, O-O 2.3 Å, B-B 2.5 Å, Zn-B 2.7 Å, Mo-Zn 2.8 Å, Zn-Zn 2.9 Å, Mo-B 3.0 Å and Mo-Mo 3.1 Å.

4.2. RMC results

From the RMC simulation several first and second neighbor partial atomic pair-correlation functions, $g_{ij}(r)$ and coordination number distributions, CN_{ij} have been revealed with a fairly good stability and statistics. Figure 5 presents $g_{B-O}(r)$, $g_{Mo-O}(r)$, $g_{Zn-O}(r)$ and $g_{O-O}(r)$ partial correlation functions for the different concentrations.
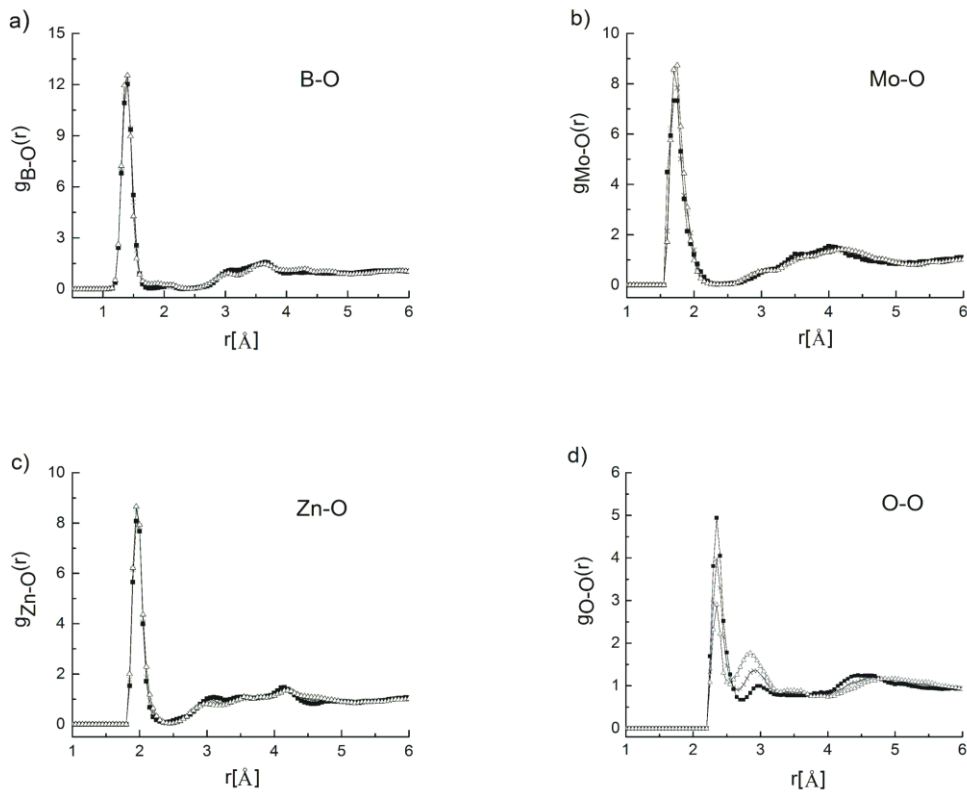

Figure 5. Partial pair distribution functions for $10MoO_3-50ZnO-40B_2O_3$(square), $20MoO_3-50ZnO-30B_2O_3$(cross) and $30MoO_3-50ZnO-20B_2O_3$ (triangle) glasses.

The first neighbor distances were calculated by Gaussian-fit (a)-(c) with a relative small error, as they are tabulated in Table 2.

Table 2. First and second neighbour distances, r_{ij}(Å) for the different atom pairs. The actual error is indicated in bracket (Å), as estimated from the data analyses of different RMC runs.

	Interatomic distances, r_{ij} (Å)									
	Atom pairs									
Sample	B-O	Mo-O	Zn-O	O-O	B-B	B-Zn	Mo-Zn	Zn-Zn	Mo-B	Mo-Mo
	(±0.01)	(±0.01)	(±0.01)	(±0.02)	(±0.05)	(±0.05)	(±0.05)	(±0.05)	(±0.05)	(±0.05)
$10MoO_3-50ZnO-40B_2O_3$	1.39	1.72	1.97	2.35/2.95	2.60	2.85	2.90	3.05	3.10	3.15
$20MoO_3-50ZnO-30B_2O_3$	1.39	1.72	1.97	2.35/2.95	2.60	2.85	2.90	3.05	3.10	3.20
$30MoO_3-50ZnO-20B_2O_3$	1.38	1.74	1.97	2.35/2.85	2.70	2.84	2.90	3.06	3.10	3.20

The B-O first neighbor distance shows slight concentration dependence, it changes from 1.38 Å to 1.39 Å with increasing boron content, which is in good agreement with our direct experimental observation obtained from the total distribution function, $G(r)$ (see Figure 4) and with our previous result reported for MoNdB-oxide glass (r_{B-O}=1.40 Å [18]). The Mo-O distance shows a slight decrease

from 1.74 Å to 1.72 Å with decrease of molybdenum content, the actual value is in accordance with other studies containing MoO_3 (r_{Mo-O}=1.75 Å [18], 1.77 Å [34], 1.76-1.78 Å [35]). The Zn-O distance appears at significantly higher value, at 1.97 Å for all three investigated samples. This value is in good agreement with the results obtained for other glasses with ZnO (r_{Zn-O}=1.93-1.95 Å [23], 1.83-1.91 Å [25], 1.94-1.97 Å [36], 1.96 Å [37]). The O-O correlation functions consist of double peak with characteristic distances at 2.35 Å and at 2.85-2.98 Å, the actual value of the second sub-peak depends on MoO_3/B_2O_3 fraction. The intensity of both O-O "sub-peaks" depends on concentration. It is remarkable, that with increasing boron content the intensity of the first peak increases, while the intensity of the second one increases with the increase of Mo-content. This observation suggests that the first sub-peak originates mainly from the O-O distance formed by the boron-oxygen units, with a similar value as it was found in v-B_2O_3 (r_{O-O}=2.38 Å [13]) and in several alkali diborate glasses (r_{O-O}=2.37-2.39 Å [12 and therein]). The O-O second sub-peak is supposed to originate from molybdenum-oxygen units [18], however, the shift of the position to higher r-values suggests that it contains contribution from the zinc-oxygen distribution, as well.

The oxygen coordination distributions are shown in Figure 6. For B-O distributions both 3- and 4-fold coordinated oxygen surroundings have been revealed, and a small number (< 5%) of 2 oxygen neighbors, the latter is supposed to be an artificial effect of the RMC model calculation. The ratio of BO_3 and BO_4 units shows concentration dependence on B_2O_3 content.
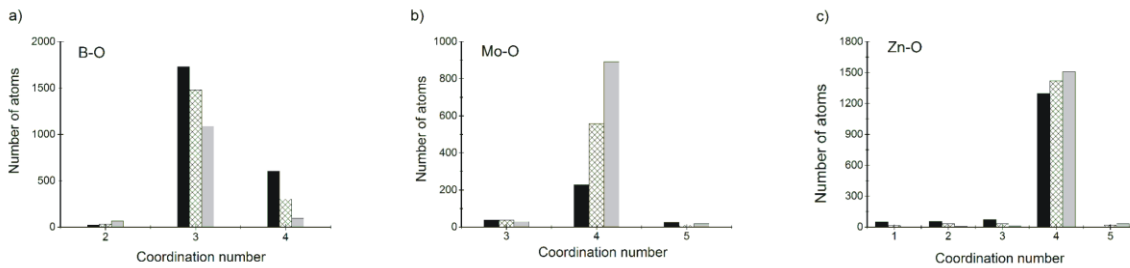

Figure 6. Oxygen coordination distributions: a) B-O, b) Mo-O, c) Zn-O where $10MoO_3$-$50ZnO$-$40B_2O_3$(black), $20MoO_3$-$50ZnO$-$30B_2O_3$(cross) and $30MoO_3$-$50ZnO$-$20B_2O_3$ (grey) glasses.

For the low boron content sample the relative number of 3-fold coordinated boron atoms is significantly higher than that for the higher boron content samples, as it is seen in Figure 6/a and from the numerical values of $BO_3/\{BO_3+BO_4\}$ and $BO_4/\{BO_3+BO_4\}$ fractions (%) (see Table 3). In consequence, the average CN_{B-O} slightly increases with increasing B_2O_3. For the Mo-O and for Zn-O coordination number distributions mainly 4-fold coordinated oxygen atoms are obtained, the number of different types of neighbors is < 5%. Note, that the coordination number distribution pattern are significantly different: for Mo-O distribution: the number of 4-fold coordinated neighbors increases in the RMC simulation box due to the increasing MoO_3 content, while for Zn-O it is constant due to the constant 50 mol% Zone content of the samples.

Table 3. Average coordination numbers, CN_{ij}(atom) and $BO_3,BO_4/\{BO_3+BO_4\}$ fraction (%) as obtained from RMC modelling. The error is about 5% as estimated from the data analyses of different RMC runs.

| Sample | Fraction (%) | | Coordination numbers, CN_{ij} (atom) | | |
| | | | Atom pairs | | |
	BO_3	BO_4	B-O	Mo-O	Zn-O
$10MoO_3$-$50ZnO$-$40B_2O_3$	74	26	3.3	3.9	3.8
$20MoO_3$-$50ZnO$-$30B_2O_3$	83	17	3.2	3.9	3.9
$30MoO_3$-$50ZnO$-$20B_2O_3$	92	8	3.1	3.9	4.0

The calculated average Co_{mo-O} and Co_{nan-O} are ~ 4 atoms, as shown in Table 3. It can be concluded that tetrahedral MO_4 and ZnO_4 units are formed, which is especially interesting for Zn-O coordination.

The RMC modeling also provides information on the second coordination sphere. Significant atomic correlations have been established from the second neighbor distribution functions, as illustrated in Figure 7. The analyses of distances between metal-metal atoms are: Mo-Zn (2.90 Å), Zn-Zn (3.05 Å), Mo-Mo (3.15 Å), between boron-metal are: B-Zn (2.85 Å), B-Mo (3.10 Å) and B-B (2.60 Å) (see Table 2).
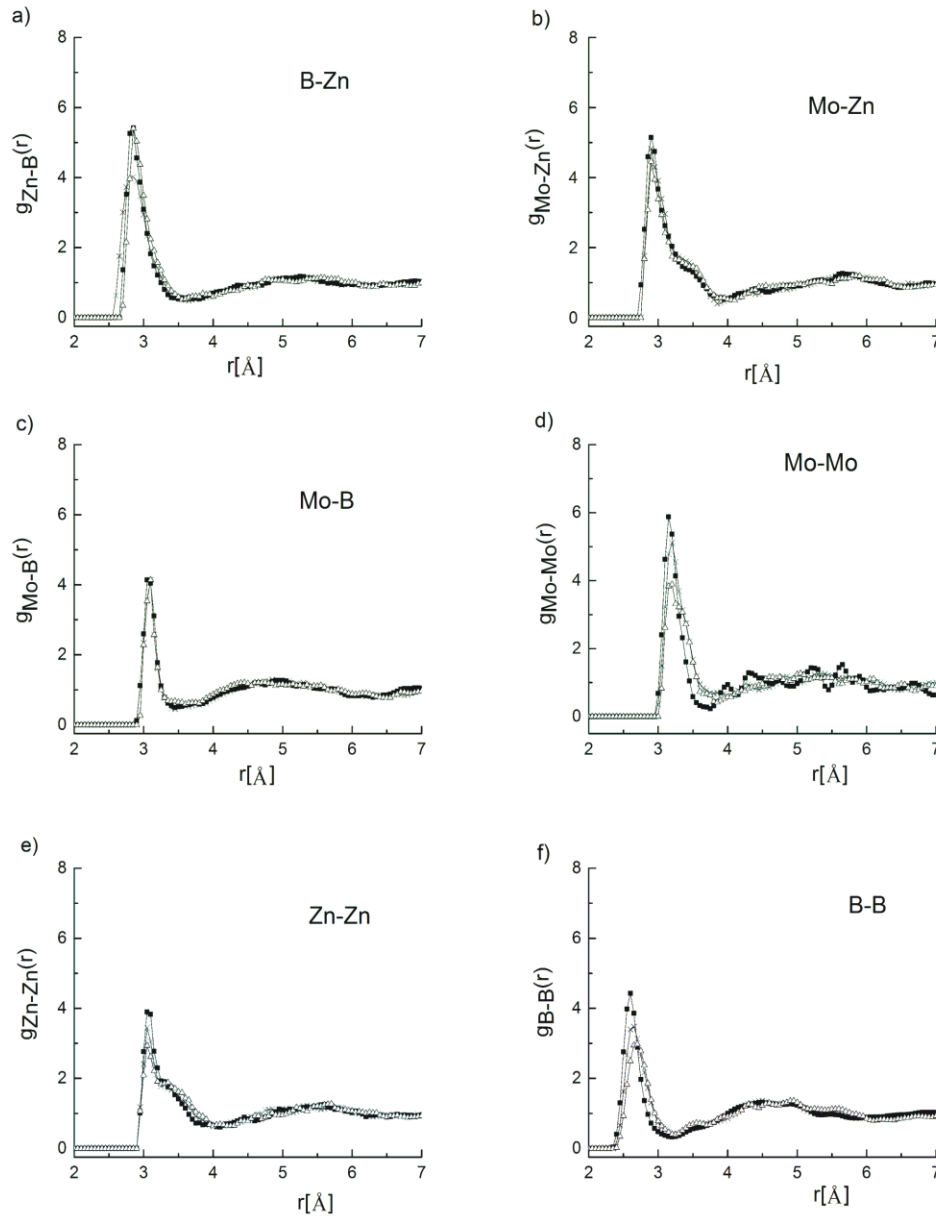

Figure 7. Second neighbour distribution functions for $10MoO_3$-$50ZnO$-$40B_2O_3$(square), $20MoO_3$-$50ZnO$-$30B_2O_3$(cross) and $30MoO_3$-$50ZnO$-$20B_2O_3$ (triangle) glasses.

5. Discussion

We have established from the RMC modeling that the basic structural units are trigonal BO_3 and tetrahedral BO_4, MoO_4 and ZnO_4 groups, and a significant correlation exists between these units. Here we focus our interest on the analysis of bond-linkages forming the medium-range structure.

As far as, the network former groups are linked through O^{2-} ions, we have calculated the oxygen centered O-B, O-Mo, O-Zn coordination number distributions. In the literature little interest has been

directed to the examination of the oxygen neighborhood with respect to network formers, as far as we know, although this may be highly informative. The results are shown in Figure 8.
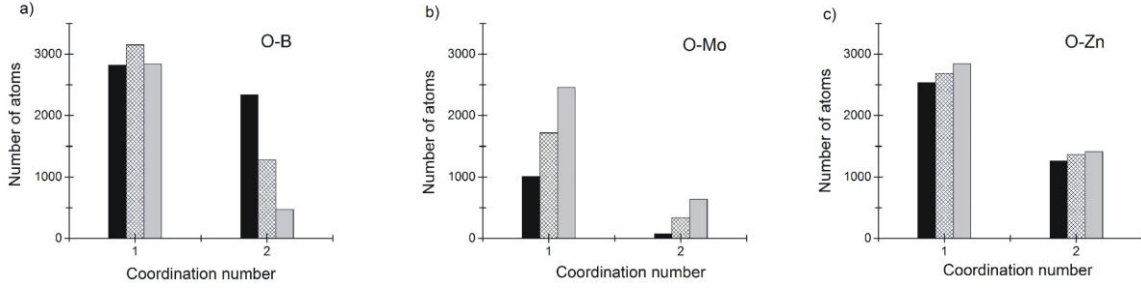

Figure 8. Oxygen centred coordination number distributions a) O-B, b) O-Mo, c) O-Zn where $10MoO_3-50ZnO-40B_2O_3$(black), $20MoO_3-50ZnO-30B_2O_3$(cross) and $30MoO_3-50ZnO-20B_2O_3$ (grey) glasses.

O^{-2} ions may be linked to 2 identical atoms, namely B-O-B, Mo-O-Mo, Zn-O-Zn or to 2 different types of atoms, namely B-O-Zn, B-O-Mo, Mo-O-Zn. We have calculated the relative number (fraction %) of the two types of linkages, the results are tabulated in Table 4. The average O-B, O-Mo and O-Zn coordination numbers are also included in Table 4.

Table 4. Average coordination numbers, CN_{ij}(atom) and relative number (fraction %) of O^{-2} ions linked to different neighbours, denoted by **1** or to identical neighbours, denoted by **2**, as obtained from RMC modelling.

Sample	O-B		CN_{O-B}	O-Mo		CN_{O-Mo}	O-Zn		CN_{O-Zn}
	Fraction (%)			Fraction (%)			Fraction (%)		
	1	**2**		**1**	**2**		**1**	**2**	
	B-O-Mo, Zn	B-O-B		Mo-O-B,Zn	Mo-O-Mo		Zn-O-B,Mo	Zn-O-Zn	
$10MoO_3-50ZnO-40B_2O_3$	55	45	1.45	93	7	1.07	67	33	1.33
$20MoO_3-50ZnO-30B_2O_3$	71	29	1.29	84	16	1.16	66	34	1.34
$30MoO_3-50ZnO-20B_2O_3$	86	14	1.14	79	21	1.21	67	33	1.33

We have found concentration dependence for O-B and O-Mo coordination distributions, while no change was established for O-Zn. The fraction of O^{-2} ions linked to **1** Zn^{2+} cation is 67% (Zn-O-B,Mo), while 33% is linked to **2** Zn^{2+} (Zn-O-Zn). As far as, in all samples the ZnO concentration is 50 mol %, whereas MoO_3/B_2O_3 changes, we can conclude that the linkages of ZnO_4 units do not have significant preference neither to boron nor to molybdenum. RMC analyses of the experimental data have shown that the Zn-O bond length is 1.97 Å for all types of linkages, namely for Zn-O-Zn, Zn-O-Mo or Zn-O-B, independently from the type of linkages of the tetrahedral ZnO_4 units. These results also support that ZnO exhibit network former property.

For O-Mo distribution we obtain, that for the lowest MoO_3 content sample the fraction of Mo-O-B,Zn mixed linkages is 93%, and Mo-O-Mo linkage is only 7%. With the increase of molybdenum content the fraction of MoO_4-MoO_4 linkages increases to 21%, while the mixed linkages decrease to 79%. It can be concluded, that MoO_4 units prefer to link to other type units. With increasing MoO_3 concentration appears an excess of oxygen, which induces formation of Mo-O-Mo linkages and could appear a "molybdenum-oxygen" framework, typical $Mo_2O_7^{2-}$ ditetrahedral groups. Our RMC calculations have shown that the Mo-O distances are the same for the MoO_4 tetrahedral units and the $Mo_2O_7^{2-}$ ditetrahedral groups within limit of error, in good agreement with the results reported in ref. [34].

The interpretation of O-B coordination distribution is more complicated, as far as, both trigonal BO_3 and tetrahedral BO_4 groups are present. In the literature it is widely discussed that BO_3 is usually

linked in boroxol ring or in single triangle BO_3 [13, 38], while mixed BO_3 and BO_4 units form well defined and stable polyborate groupings, which also occur in borate crystals, i.e. (di)-triborate, metaborate, (di and tri)-pentaborate superstructural units [9-11]. Table 4 shows, that more than 50% of boron atoms are linked to MoO_4 or ZnO_4 (O-B column **1**), and concentration dependence can be observed. The number of B-O-B linkages (O-B column **2**) significantly decreases from 45% to 14% with increasing MoO_3/B_2O_3. This means, that the boron centered units prefer the linkage to MoO_4 or ZnO_4. The analysis of the results for BO_3 and BO_4 fraction (see Table 3) shows that the relative number of BO_3 significantly increases from 74% up to 92% with increasing MoO_3/B_2O_3. From these observations we may conclude that only small amount of boroxol ring is formed in the network structure (in that case B-O-B bond-linkages should be observed). We suppose that the network is formed by BO_3 and BO_4 organized into superstructure units, and partly by separated BO_3 triangles. They are linked to MoO_4 or ZnO_4, forming in this manner mixed bond-linkages.

In some aspect, similarity may be found with our previous interpretation of the multi-component borosilicate glasses [39], where we have established mixed network structure including [3]B-O-[4]Si and [4]B-O-[4]Si chain segments. In the present system the oxygen centered coordination number distributions show that most of Mo atoms favor to be connected through an oxygen to Zn and B atoms, and the majority of the Zn atoms prefers to be linked to B or Mo atoms forming in this way [4]Mo-O-[3]B, [4]Mo-O-[4]B, [4]Mo-O-[4]Zn, [3]B-O-[4]Zn, [4]B-O-[4]Zn linkages.

6. Conclusions

Neutron diffraction study has been performed on $xMoO_3$-50ZnO-(50-x)B_2O_3, x=10, 20, 30 mol% glasses, and the experimental data were simulated by reverse Monte Carlo modeling. The first- and second neighbor correlation functions, atomic distances and coordination numbers have been revealed, not yet reported for this system. It was found, that the first neighbor distances do not depend on concentration within error of limit, the actual values are r_{B-O}=1.38 Å, r_{Mo-O}=1.72 Å and r_{Zn-O}=1.97 Å. ZnO proved to be a network former, not a modifier as it is often reported in the literature for similar systems. From the analyses of the obtained structural parameters we have concluded that the glassy network is formed by trigonal BO_3 and tetrahedral BO_4, MoO_4, ZnO_4 groups. Concentration dependence was found for the BO_4/BO_3 fraction, it increases with increasing B_2O_3 content. We have concluded that only small amount of boroxol ring is present and it is supposed that the network is formed by organization of BO_3 and BO_4 groups into superstructure units, and partly by separated BO_3 triangles. The BO_3 and BO_4 units are linked to MoO_4 or ZnO_4, forming mixed [4]Mo-O-[3],[4]B, [4]Mo-O-[4]Zn, [3],[4]B-O-[4]Zn bond-linkages. Significant medium-range order exists up to ~7 Å.

References

1. L. Aleksandrov, T. Komatsu, R. Iordanova and Y. Dimitriev, „Structure study of MoO_3-ZnO-B_2O_3 glasses by Raman spectroscopy and formation of α-$ZnMoO_4$ nanocrystals," *Optical Materials* **33** [6], 839-845 (2011).
2. L. Alexandrov, R. Iordanova, Y. Dimitriev, K. Hamda, J. Ide and M. Milanova, „Glass Formation in the MoO_3-La_2O_3-Nd_2O_3 System," *Advanced Materials Research* **39-40** 37-40 (2008).
3. L. Alexandrov, R. Iordanova and Y. Dimitriev, "Glass formation in the MoO_3-Nd_2O_3-La_2O_3-B_2O_3," *J. Non-Cryst. Solids* **355** 2023-2026 (2009).

4. L. Alexandrov, R. Iordanova and Y. Dimitriev, „Glass formation in the MoO_3-La_2O_3-B_2O_3 system," *Phys. Chem. Glasses: European J. Glass Sci. Technol. B.* **48** [4] 242-245 (2007).

5. Y. Dimitriev, R. Iordanova, L. Aleksandrov and K. L. Kostov, „Boromolybdate glasses containing rare earth oxides," *Phys. Chem. Glasses: European J. Glass Sci. Technol. B.* **50** [3] 212-218 (2009).

6. Y. Dimitriev and R. Iordanova, „Non-traditional molybdate glasses," *Phys. Chem. Glasses: European J. Glass Sci. Technol. B.* **50** [2] 123-132 (2009).

7. R. Iordanova, L. Aleksandrov, A. Bachvarova-Nedelcheva, M. Ataala and Y. Dimitriev, "Glass formation and structure of glasses in B_2O_3-Bi_2O_3-MoO_3 system," *J. Non-Cryst. Solids* **357** 2663-2668 (2011).

8. L. Aleksandrov, T. Komatsu, R. Iordanova and Y. Dimitriev, "Study of molybdenum coordination state and crystallization behavior in MoO_3-La_2O_3-B_2O_3 glasses by Raman spectroscopy," *Journal of Physics and Chemistry of Solids* **72** 263-268 (2011).

9. A. C. Wright, J. L. Shaw, R. N. Sinclair, N. M. Vedishcheva, B. A. Hakhmatkin and C. R. Scales, „The use of crystallographic data in interpreting the correlation function for complex glasses," *J. Non-Cryst. Solids* **345-346** 24-33 (2004).

10. A. C. Wright, R. N. Sinclair, C. E. Stone and J. L. Shaw, "A neutron diffraction study of $2M_2O.5B_2O_3$ (M=Li, Na, K, Rb, Cs & Ag) and $2MO.5B_2O_3$ (M=Ca & Ba) glasses," *Phys. Chem. Glasses Eur. J. Glass Sci. Technol. B* **53** 191-204 (2012).

11. N. Barrow, Superstructural units in lithium borate glasses, Department of Physics, University of Warwick, Coventry, CV4 7AL, 2006.

12. N. Ohtori, K. Takase, I. Akiyama, Y. Suzuki, K. Handa, I. Sakai, Y. Iwadate, T. Fukunaga and N. Umesaki, "Short-range structure of alkaline-earth borate glasses by pulsed neutron diffraction and molecular dynamics simulation," *J. Non-Cryst. Solids* **293-295** 136-145 (2001).

13. M. Fábián, E. Sváb, Th. Proffen and E. Veress, "Neutron diffraction and reverse Monte Carlo modelling of v-B_2O_3 and $75B_2O_3$–$25Na_2O$ glasses," *J. Non-Cryst. Solids* **356** 441-446 (2010).

14. M. Fábián, E. Sváb and M. v. Zimmermann, „Structure study of new uranium loaded borosilicate glasses," *J. Non-Cryst. Solids* **380** 71-77 (2013).

15. S. K. Lee, K. Mibe, Y. Fei, G. D. Cody and B. J. Mysen, "Structure of B2O3 Glass at High Pressure: A ^{11}B Solid-State NMR Study," *Physical Review Letters* **94** 165507(2005).

16. D. Lin-Shu and J. F. Stebbins, „Solid-state NMR study of metastable immiscibility in alkali borosilicate glasses," *J. Non-Cryst. Solids* **315** [3] 239-255 (2003).

17. O. Bouty, J. M. Delaye, B. Beuneu and T. Charpentier, „Modelling borosilicate glasses of nuclear interest with the help of RMC, WAXS, neutron diffraction and ^{11}B NMR," *J. Non-Cryst. Solids* **401** 27-31 (2014).

18. M. Fabian, E. Svab and K. Krezhov, „Neutron diffraction and RMC modeling of new amorpous molybdate system," *Journal of Physics:Conference Series* **558** 012017 (2014).

19. G. Calas, M. Le Grand, L. Galoisy and D. Ghaleb, „Structural role of molybdenum in nuclear glasses: an EXAFS study," *Journal of Nuclear Materials* **322** [1] 15-20 (2003).

20. J. Subcik, L. Koudelka, P. Mosner, L. Montagne, B. Revel and I. Gregora, „Structure and properties of MoO_3-containing zinc borophosphate glasses," *J. Non-Cryst. Solids* **355** [16-17] 970-975 (2005).

21. U. Hoppe, G. Walter, R. Kranold, D. Stachel and A. Barz, „The dependence of structural peculiarities in binary phosphate glasses on their network modifier content," *J. Non-Cryst. Solids* **192-193** 28-31 (1995).

22. U. Hoppe, G. Walter, D. Ilieva, G. Carl and J. Neuefeind, „Me-O coordination numbers in Ga and Zn phosphate glasses from meta- to pyrophosphate compositions-a high-energy X-ray diffraction study,"http://hasyweb.desy.de/science/annual_reports/2001_report/part1/contrib/44/4829 (2001).

23. D. A. McKeown, I. S. Muller, A. C. Buechele and I. L. Pegg, „Local environment of Zn in zirconium borosilicate glasses determined by X-ray absorption spectroscopy," *J. Non-Cryst. Solids*

261 [1-3] 155-162 (2000).

24. D. Saritha, Y. Markandeya, M. Salagram, M. Vithal, A. K. Singh and G. Bhikshamaiah, „Effect of Bi_2O_3 on physical, optical and structural studies of ZnO-Bi_2O_3-B_2O_3 glasses," J. *Non-Cryst. Solids* **54** 5573-5579 (2008).

25. S. Rada, P. Pascuta, L. Rus, M. Rada and E. Culea, „Spectroscopic properties and ab initio calculations on the structure of erbium-zinc-borate glasses and glass ceramics," *J. Non-Cryst. Solids* **358** 30-35 (2012).

26. R. L. McGreevy and L. Pusztai, "Reverse Monte Carlo Simulation: A New Technique for the Determination of Disordered Structures," *Mol. Simul.* **1** 359-367 (1988).

27. National Institute of Materials Physics, Bucharest, Romania, http://lab50.infim.ro/tem.htm#

28. Slovenian NMR Centre, http://www.nmr.ki.si/600_magnet.html

29. E. Sváb, Gy. Mészáros and F. Deák, „Neutron powder diffractometer at the Budapest research reactor," *Materials Science Forum* **228** 247-252(1996); http://www.bnc.hu/

30. J. P. Ambroise, M. C. Bellissent-Funel and R. Rellissent, „Neutron scattering determination of local order in amorphous and liquid systems using a position sensitive detector," *Rev. Phys. Appl.* **19** 731-734 (1984); http://www-llb.cea.fr/en/

31. A.C. Hannon, „ISIS Disordered Materials Database," http://www.isis.stfc.ac.uk/groups/disordered-materials/database/ (2006).

32. Reverse Monte Carlo homepage, http://www.szfki.hu/~nphys/rmc++/opening.html

33. L. Alexandrov, private communication.

34. M. Rada, S. Rada, P. Pascuta and E Culea, "Structural properties of molybdenum-lead-borate glasses," *Spectrochimia Acta Part A* **77** 832-837 (2010).

35. D. Caurent, O. Majerus, E. Fadel, A. Quintas, C. Gervais, T. Charpentier and J. Neuville, "Structural investigations of borosilicate glasses containing MoO_3 by MAS NMR and Raman spectroscopies," *Journal of Nuclear Materials* **396** 94-101 (2010).

36. K. Suzuya, K. Itoh, A. Kajinami and C. K. Loong, "The structure of binary zinc phospate glasses," *J. Non-Cryst. Solids* **345-346** 80-87 (2004).

37. G. Calas, L. Cormier, L. Galoisy and P. Jollivet, "Structure-property relationships in multicomponent oxide glasses," *Comptes Rendus Chimie* **5** 831-843 (2002).

38. C. Joo, U. Werner-Zwanziger and J. W. Zwanziger, „The ring structure of boron trioxide glass," *J. Non-Cryst. Solids* **261** 282-286 (2000).

39. M. Fabian, E. Svab, Th. Proffen and E. Veress, "Structure study of multi-component borosilicate glasses from high-Q neutron diffraction measurement and RMC modeling," *J. Non-Cryst. Solids* **354** 3299-3307 (2008).